BioComm: Biocompatible Physical Layer Design for Wireless Intra-Body Communications

Pedram Johari, *Member, IEEE*, Hadeel Elayan, *Member, IEEE*, and Josep M. Jornet, *Fellow, IEEE*

***Abstract*—*In-vivo* Wireless Nanosensor Networks (iWNSNs) consist of nano-sized communicating devices with unprecedented sensing capabilities that operate inside the human body in real-time. The current state-of-the-art in nanoelectronics and nanophotonics points to the Terahertz (THz) band (0.1–10 THz) and the optical frequency bands (infrared, 30-400 THz, and visible, 400-750 THz) as the promising spectral bands for nanosensor communications. In this paper, we propose and analyze a biocompatible modulation technique for iWNSNs. A mathematical framework is formulated to optimize the parameters of an adaptive Time Spread On-Off Keying (OOK) pulse-based modulation. This optimization considers both the physics of the intra-body optical channel and the light-matter interactions, along with the resulting photo-thermal effects in biological tissues. The outcomes of the analytical optimization model are validated through extensive numerical simulations. The results highlight a trade-off between link efficiency and the biocompatibility of the transmitted signals. Numerical analysis shows that the proposed biocompatible modulation technique can easily achieve a Bit Error Rate (BER) of 10^{-2} before coding, within the bio-safety measures, indicating a reliable intra-body channel for data transmission. This means that the channel can effectively convey information, such as health monitoring data or control signals for medical devices, without significant data loss or corruption.**

***Index Terms*—Intra-body wireless communications, biocompatible modulation, in-vivo wireless nanosensor networks, terahertz and optical communications, Internet of Nano Things (IoNT).**

I. Introduction

NANOTECHNOLOGY is facilitating the creation of innovative nanosensors capable of detecting various events at the nanoscale with remarkable precision. Recently, there have been proposals for nano-sensing and nano-actuating systems designed for *in-vivo* applications, operating within the human body in real-time. These emerging systems hold the potential to revolutionize disease diagnosis and treatment by offering faster and more accurate results compared to traditional technologies [1], [2], [3]. Moreover, they open the door to novel brain-computer interfaces with unprecedented applications in the fields of biology and medicine [4]. Presently, researchers have successfully utilized surface plasmon resonance (SPR) sensors to analyze circulating biomarkers in body fluids, contributing to the diagnosis of severe diseases, including various cardiovascular and neuronal conditions [5], [6]. By immobilizing biomarker-specific capture molecules on the sensor surface, binding events between these molecules and circulating biomarkers in the sample can be detected. The resulting change in refractive index near the sensor surface leads to a measurable shift in the SPR signal, enabling quantitative analysis of biomarker concentrations. SPR sensors can also determine biomarker binding kinetics and allow for multiplexing, facilitating simultaneous detection of multiple biomarkers. This capability is invaluable in clinical diagnostics and biomedical research for monitoring disease progression, treatment efficacy, and biomarker dynamics in response to stimuli. More recently, these sensors have been employed to directly detect different types of cancer from blood samples [7], [8].

Through communication capabilities, nanosensors will autonomously transmit their sensing information to a central repository, be directed from a command center, or collaborate in joint actions as necessary. The resulting *in-vivo* Wireless Nanosensor Networks (iWNSNs) form the foundation of transformative smart healthcare systems. In contrast to existing nano-biosensing systems, which rely on external measuring equipments and require the intervention of a doctor, iWNSNs are anticipated to facilitate the seamless transmission of information from inside to outside the body, as demonstrated in Fig. 1.

The state of the art in nano-electronics and nano-photonics points to the Terahertz (THz) band, ranging from 0.1–10 THz, and the optical frequency bands (infrared, 30-400 THz, and visible, 400-750 THz) as the frequency range for communication among nano-biosensors. Among different technologies, plasmonic nanolasers with sub-micrometric footprint [9], [10], plasmonic nano-antennas capable of confining light in nanometric structures [11], [12], and single-photon detectors with unrivaled sensitivity [13], [14], have been suggested to enable communication among implanted nanosensors.

When designing communication algorithms for iWNSNs, two fundamental aspects must be considered. First and foremost, the intra-body channel significantly influences the propagation of optical signals. From the nanosensor perspective, the body consists of various elements such as cells, organelles, proteins, and molecules, each with distinct geometry, arrangement, and electromagnetic (EM) properties.

Manuscript received 21 May 2024; accepted 26 June 2024. Date of publication 4 July 2024; date of current version 25 September 2024. This work was supported by the U.S. National Science Foundation (NSF) under Grant IIP-1718177 and Grant CBET-1706050. The associate editor coordinating the review of this article and approving it for publication was S. Abadal. *(Corresponding author: Hadeel Elayan.)*

The authors are with the Department of Electrical and Computer Engineering, Northeastern University, Boston, MA 02115 USA (e-mail: p.johari@northeastern.edu; hadeel.mohammad@mail.utoronto.ca; j.jornet@northeastern.edu).

Digital Object Identifier 10.1109/TMBMC.2024.3423021

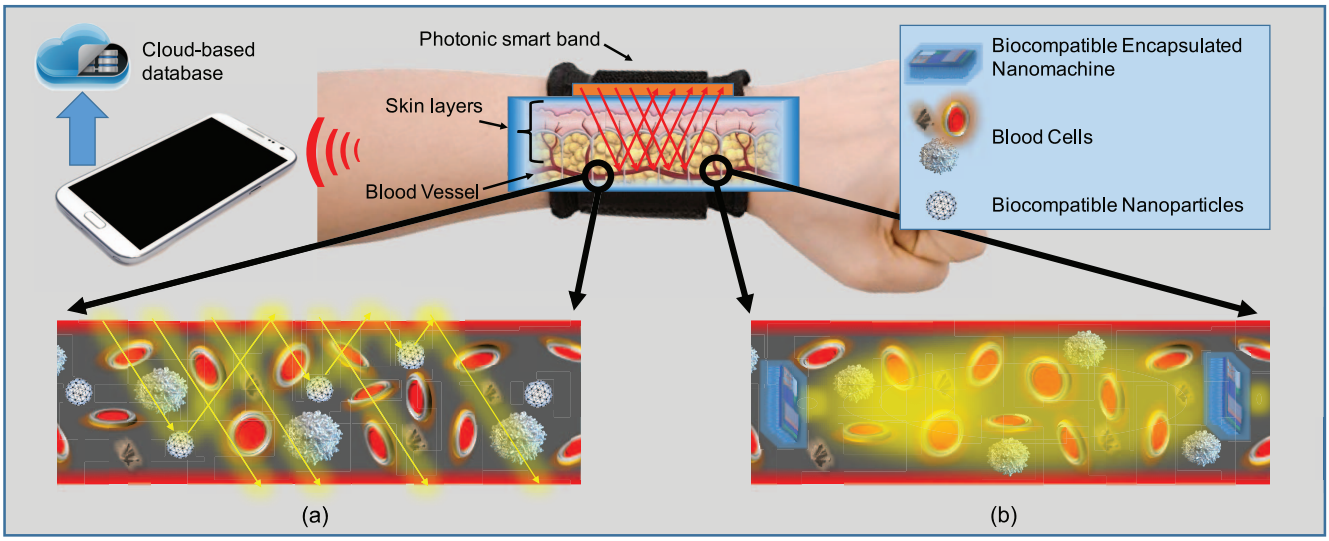

Fig. 1. System model (a) communication channel between a subcutaneously implanted biophotonic nano-chip and floating passive nanoparticles in the circulatory system (b) communication channel between active nanomachines floating inside a blood vessel.

Despite the challenges in predicting the propagation of optical signals within biological tissues, recent theoretical [15], [16] and experimental [17], [18] studies have demonstrated that some cells behave as optical lenses, enhancing the propagation distance of optical signals in biological environments. Alternatively, the use of the THz band, which exhibits comparatively lower penetration loss in intra-body communications, has recently attracted interest among researchers [19], [20]. While employing the THz band has the potential to increase communication distance, i.e., decrease path loss, it also poses a risk of causing tissue damage if the transmission power exceeds tolerable radiation thresholds. This raises the second primary concern in developing intra-body communication models.

In general, the radiation and propagation of EM waves inside the human body can induce photo-thermal effects on biological tissues, potentially leading to undesirable damage. EM waves initiate internal vibrations in molecules. As these molecules are confined within a liquid or solid structure and cannot freely move, the vibrational energy transforms into friction, generating heat. Although this process underlies some healing mechanisms involving resonant nanoparticles [21], it becomes undesired when the goal is reliable information transmission among nanosensors or to off-body devices. Despite the expectation of relatively low information volumes in iWNSNs, efficient communication is essential to prevent unnecessary energy radiation. Consequently, new communication techniques must be developed to avert potential harm to biological tissues based on the photosensitivity of the target tissues.

When comparing THz and optical signals, recent studies have indicated that optical signals exhibit a less harmful photo-thermal impact on biological tissues [22], [23]. However, due to higher propagation losses compared to THz radiation [19], more power is required to achieve a similar communication distance with optical waves, potentially leading to increased heat generation. Therefore, to ensure the biocompatibility of intra-body EM communications, it is imperative to first comprehend the trade-offs and then control fundamental light-matter interactions from the cellular to the tissue level. Throughout this paper, the term *light-matter interaction* is used for both visible optical waves and THz band radiations.

In this study, we introduce a biocompatible modulation technique for iWNSNs. Specifically, we develop a mathematical framework to optimize the parameters of an adaptive Time Spread On-Off Keying (TS-OOK) pulse-based modulation. The optimization takes into account the physics of the intra-body channel and interactions in biological tissues, considering the resulting photo-thermal effects. To achieve this, we formulate and solve an optimization problem aimed at minimizing the impact of EM waves while meeting the minimum Quality of Service (QoS) requirements of the intra-body communication channel. We employ the Bit Error Rate (BER) as the QoS measure to assess the overall performance and reliability of communication within the iWNSN. Furthermore, we validate the proposed modulation technique and the analytical optimization model through extensive numerical simulations in an optical communication scenario.

The results presented in this paper highlight a trade-off between link efficiency and the biocompatibility of transmitted signals, where we identify optimal modulation parameters. It's noteworthy that, in this study, we advocate for optical intra-body communications and focus our numerical analysis accordingly. Nevertheless, the proposed framework can be generally applied for nanoscale intra-body communications at other frequencies. For instance, in the case of THz frequencies, the system can be adjusted by considering multiple RBCs as well as integrating the corresponding parameters into the proposed model.

The remainder of the paper is organized as follows. In Section II, a complete system architecture and a channel model for intra-body wireless communication are presented. In Section III, the impact of EM wave propagation on heat

generation in biological tissues is studied, and a biocompatible modulation technique for intra-body communications is proposed. In Section IV, we formulate and solve an optimization problem with the objective of minimizing the temperature increase in biological tissues while maintaining the minimum QoS requirements by using the proposed modulation technique. Section V contains a numerical study of the results. Finally, we conclude the paper in Section VI.

II. System Architecture and Communication Channel Model

A. Naonophotonic Smart Band and Nanomachines

The communication channel between two nanosensors in an iWNSN is considered. Fig. 1 illustrates two possible scenarios for intra-body communication. In scenario (a), a nanophotonic smart wristband communicates with subcutaneously implanted or floating nanoparticles in blood vessels. The nanophotonic smart band contains an array of optical nano-sources and detectors for the distributed excitation and measurement of light transmitted through the skin layers and eventually reflected back from the implant/nanoparticles. Since the implants/nanoparticles are passive devices, this architecture allows for moving all the active components of the system outside the human body and serves as a nano-to-macro interface between bio-events and the user.

In a more futuristic scenario, as illustrated in Fig. 1(b), we contemplate injectable/implantable nanomachines capable of performing simple tasks such as biosensing, basic computation, or even local actuation inside the human body. Fig. 2 portrays a nanomachine encapsulated with a biocompatible material and comprising active and passive electronic elements. Notably, it features a nano-transceiver, nanolaser, and nano-antenna, enabling communication with other nanomachines and the wearable smart band through EM signals. Additionally, the nanomachines incorporate energy harvesting circuitry that replenishes the energy stored in a tiny nano-battery. Through this energy harvesting mechanism, circulating nanomachines can overcome their energy bottleneck and potentially have an infinite lifetime, given the joint design of energy harvesting and consumption processes [24], [25], [26], [27].

In Fig. 2, the energy stored in the nano-battery can be calculated as [24]

$$\mathcal{E}_{cap}\left(n_{cycle}\right) = \frac{1}{2} C_{cap} \left(V_{cap}\left(n_{cycle}\right)\right)^2, \tag{1}$$

where the n_{cycle} is the number of compress-release cycles of the piezoelectric nanowire array which generates the current used to charge the nanocapacitor. C_{cap} is the total capacitance of the nanocapacitor and V_{cap} is the total stored voltage in the capacitor (or equivalently in the battery) which can be computed as [24]

$$V_{cap}\left(n_{cycle}\right) = V_s \left(1 - e^{\left(-\frac{n_{cycle}\, t_{cycle}}{R_s\, C_{cap}} \right)} \right). \tag{2}$$

Here, t_{cycle} is the cycle length, V_s and R_s are the Thevenin's equivalent voltage and resistor of the piezoelectric nanogenerator (including the rectifying circuit). As it can be seen from (2), the maximum storable voltage in the capacitor is V_s; therefore, the maximum available energy that can be stored in the nanomachine is given as

$$\mathcal{E}_{max} = max\{\mathcal{E}_{cap}\left(n_{cycle}\right)\} = \frac{1}{2} C_{cap}\, V_s^2. \tag{3}$$

It can be observed from (1) and (2) that the energy harvesting is a time consuming process and the availability of the energy at any given point of time depends on the communication speed and the energy consumption rate [25]. However, in our work, we assume that the nanomachine has enough time before each transmission to store the maximum possible energy. Further details regarding this point will be given in Section III-D.

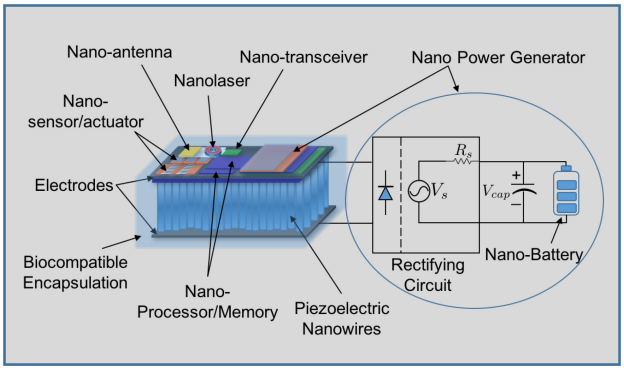

Fig. 2. Structure of a nanomachine with energy harvester circuitry.

B. EM Wave Propagation Inside the Human Body

From the nanomachine's perspective in an iWNSN, biological tissues are a collection of different types of elements, such as cells, organelles, and molecules, each with different EM properties. In both scenarios depicted in Fig. 1, EM signals need to penetrate skin, fat, and blood vessels to reach either the passive implants and nanoparticles or the active nanomachines. Various analytical and empirical models have been derived to capture the EM propagation patterns inside biological tissues [28], [29], [30], [31]. In [15], an analytical channel model was proposed for intra-body biosensing, where the properties of individual cells are considered rather than treating different tissues as homogeneous materials. Given the accuracy and relevance of this model to our scenario, we adopt the same model in this paper to define the propagation loss of EM waves radiated through an assembly of cells. This is mathematically expressed as

$$\mathcal{L}(d) = 10 \log \frac{P_{ant}}{P_{rx}(d)} = 10 \log \frac{8\pi^2 \eta^2 |I_0 l|^2}{9 |E(d)|^2 \lambda_g^4}, \tag{4}$$

where P_{ant} is the radiated power from the antenna, $P_{rx}(d)$ is the received power at a distance d from the antenna. $\eta = \sqrt{\mu/\epsilon}$ is the wave impedance where μ and ϵ are the permeability and permittivity of the medium, respectively. I_0 is the input current passing through the antenna and l is the antenna length. In (4), $E(d)$ is the measured electric field intensity at a distance d from the transmitting antenna and λ_g

is the effective wavelength, which depends on the frequency f and the cell's refractive index n.

C. A Deeper Look Into the EM Radiation Through Single Cells

Recent research has shown that specific cell types, such as RBCs within human blood, can function as optical lenses, concentrating the radiation pattern of EM waves at a focal point beyond the cell [17]. This effect has two significant impacts: i) it increases the intensity of EM energy at the focal areas, potentially reducing path loss in a communication link; ii) the EM wave energy that cannot penetrate the cell body is partially absorbed by the cell. The absorption of EM energy in these affected areas eventually leads to heat generation, a topic we will investigate in more detail in Section III-A.

The channel impulse response depicting a scenario where a single cell lies between the transmitter and receiver is given as [32]

$$H_F(f,d) = \gamma(r) \cdot \left(|\vec{E}_F^{mr}| e^{-i\omega\tau_{mr}} + |\vec{E}_F^{fr}| e^{-i\omega\tau_{fr}} \right), \quad (5)$$

where $\gamma(r)$ is the cell size gain factor which is a function of the cell radius. This factor indicates that the larger the cell, the bigger the surface of the cell that is exposed to the incoming light, hence more energy will be focused at the focal area after the cell. In (5), $\omega = 2\pi f$ is the angular frequency, τ_{mr} and τ_{fr} are the time delays between the transmitted and received EM waves for the main and the focusing rays, respectively. Finally, $|\vec{E}_F^{mr}|$ and $|\vec{E}_F^{fr}|$ represent the intensity of the received EM wave coming through the main and the focusing rays, respectively. These intensities can be calculated from the path loss as follows

$$|\vec{E}_F^{mr}| = |\vec{E}_0| \mathcal{L}^{mr}, \quad (6)$$

$$|\vec{E}_F^{fr}(\alpha)| = \pi |\vec{E}_0| \left(\mathcal{L}^{fr,p} cos(\psi) + \mathcal{L}^{fr,s} \right). \quad (7)$$

Here, E_0 is the intensity of the transmitted EM wave, $\mathcal{L}^{mr}$ is the path loss of the main ray due to the molecular absorption and scattering, $\mathcal{L}^{fr,p}$ and $\mathcal{L}^{fr,s}$ represent the path loss that each p- and s-polarized focusing ray faces in its path to the focal point, respectively. Parameter α is the closeness factor of the focusing ray to the focal line and ψ represents the angle between the main and the focusing ray at a given focal point [32]. Equations (5) through (7) show the intensity of the EM wave after passing through a cell. This demonstrates an increase in the energy of the EM wave in a focusing area after passing through the cell, as depicted in Fig. 3. Specifically, Fig. 3 illustrates the EM wave propagation pattern through a single RBC, obtained from simulation results using COMSOL Multiphysics® [33]. As seen in the figure, the EM wave has very low intensity inside the cell. This is partially due to the absorption phenomenon, which will be discussed next.

It is to be noted that this model is utilized as the building block to simulate a more complicated channel model, which includes numerous cells of different types in multiple layers. This will allow us to obtain a more realistic model of the light propagation in a human blood vessel by considering the movements of the cells.

III. Biocompatible Modulation Technique for Intra-Body Communications

A. Heat Generation in Biological Tissues Due to EM Wave Radiation

The molecules within biological tissues become excited by EM waves at specific frequencies within the optical spectra. When this occurs, the atoms of these excited molecules start to vibrate internally, leading to the conversion of part of the energy of the propagating EM wave into kinetic energy [34]. This conversion results in two immediate outcomes. From a communication perspective, the converted energy can be regarded as the loss of propagating EM wave energy, constituting path loss. This aspect has been considered in the channel response and path loss calculation, as discussed in Sections II-B and II-C.

On the other hand, the internal vibrations of the molecules induce friction, generating heat in their immediate surroundings. If the generated heat exceeds a certain threshold, it may lead to thermal tissue damage [35], [36]. Cumulative Equivalent Minutes at 43 °C (CEM_{43}) is an accepted metric for assessing thermal exposure dose (temperature and time of exposure), which correlates well with thermal damage in various tissues [35], [37]. In this context, our main contribution is the development of a biocompatible modulation technique that ensures a level of QoS for the communication channel while maintaining the biological thermal impact below a tolerable threshold.

To find the effect of the EM wave radiation in temperature increase, we start with the heat transfer equation which is described by the following equation [38]

$$\nabla k(\mathbf{r}) \nabla T(\mathbf{r},t) + Q(\mathbf{r},t) = \rho(\mathbf{r}) \mathcal{C}(\mathbf{r}) \frac{\partial T(\mathbf{r},t)}{\partial t}, \quad (8)$$

where $T(\mathbf{r},t)$ is the temperature as a function of coordinate $\mathbf{r}$ and time t, $\rho(\mathbf{r})$, $\mathcal{C}(\mathbf{r})$ and $k(\mathbf{r})$ are the mass density, specific heat capacity and thermal conductivity, respectively. In (8), the local heat at the biological cell $Q(\mathbf{r}, t)$ is the result of the EM wave absorption which can be calculated using

$$\begin{aligned} Q(\mathbf{r},t) &= \langle \mathbf{J}(\mathbf{r},t).\mathbf{E}(\mathbf{r},t) \rangle_t \\ &= -\frac{1}{2} \Re \left[j\omega \frac{\epsilon(\mathbf{r}) - 1}{4\pi} \tilde{\mathbf{E}}(\mathbf{r}) \tilde{\mathbf{E}}^*(\mathbf{r}) \right], \end{aligned} \quad (9)$$

where $\mathbf{J}(\mathbf{r},t)$ represents the current density, $\mathbf{E}(\mathbf{r},t) = \Re[\tilde{\mathbf{E}}(\mathbf{r}).e^{-i\omega t}]$ is the resulting electric field in the cell, $\epsilon(\mathbf{r})$ is the dielectric constant of the biological tissue, $\Re$ denotes the real part of a complex number and $\langle . \rangle_t$ represent the time averaging. Once the amount of added heat (generated due to the presence of EM wave) is calculated using (9), one can find the temperature increase in the region. Note that the maximum temperature changes in a substance due to added heat is defined by the specific heat formula $\Delta T_{max} = Q/(\mathcal{C}.m)$, where m represents the mass of the tissue under study.

We use COMSOL Multiphysics® [33] to simulate heat generation in the presence of an EM wave source. Fig. 4(a) illustrates the heat generated in blood, with a single RBC as the most absorbing cell. Fig. 4(b) displays the temperature

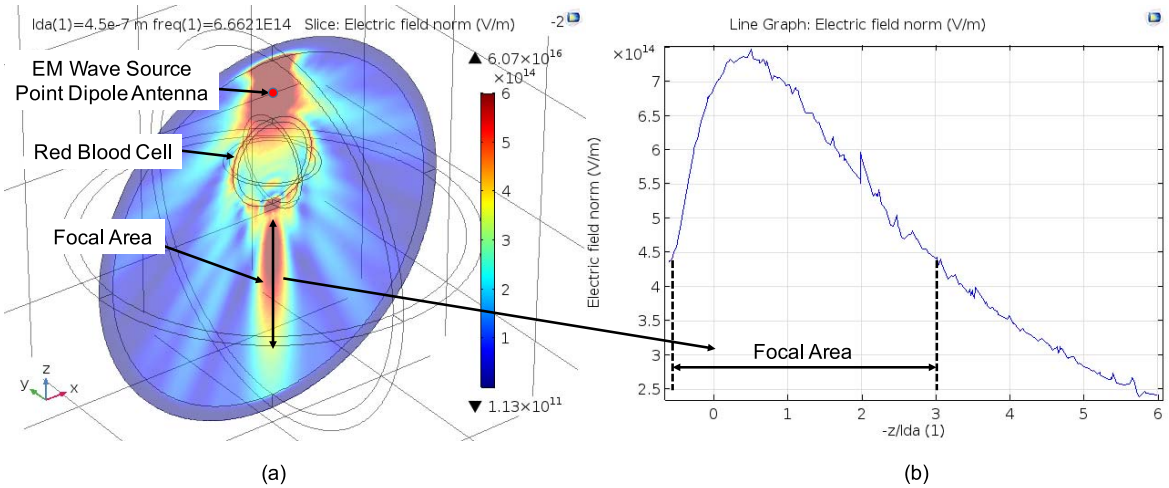

Fig. 3. Simulation of EM wave propagation through a single RBC. (a) COMSOL Multiphysics® simulation model. (b) Electric field intensity on the focal line.

increase versus time at three different points: the center of the cell, on the cell membrane, and between the cell and antenna. It is to be noted that the temperature decrease during the cool-down process is provided in Fig. 10. It is further observed from Fig. 4(b) that the temperature increase due to EM wave radiation and the subsequent temperature decrease during the cool-down process when the EM wave source is turned off can both be approximated with an exponential curve, each having different time constants. Therefore, the temperature of a given area of study at any point in time can be modeled as follows

$$T(t) = \begin{cases} T_0, & t < t_0 \\ T_0 + \Delta T_{max}\left(1 - e^{-\frac{t-t_0}{\tau_{inc}}}\right), & t_0 \le t \le t_0 + \tau_{on} \\ T(t_0+\tau_{on})e^{-\frac{t-(t_0+\tau_{on})}{\tau_{dec}}}, & t > t_0 + \tau_{on}, \end{cases} \tag{10}$$

where T_0 is the normal temperature of the body, τ_{inc} and τ_{dec} are the time constants for the temperature increase and temperature decrease, respectively, τ_{on} is the total time that the EM wave source is "ON" and in radiation mode, and t_0 is the radiation start time.

B. Proposed Biocompatible Modulation Technique

We employ a simplex communication channel using Amplitude Shift Keying (ASK) modulation known as OOK. This modulation scheme is a promising technique for iWNSNs communication for several reasons. Firstly, the processing and power limitations of nanomachines make complex modulations impractical. Secondly, the communication requirements between nanomachines involve a minimal amount of information and bandwidth, with low environmental optical noise in the human blood vessels. Hence, nanomachines can communicate through simple, small messages that do not necessitate intricate coding and modulation schemes. Lastly, due to complex changes in light polarization, as well as dispersion and scattering phenomena, detecting high-order modulation and coding schemes is impractical for tiny nanomachines with limited processing capabilities.

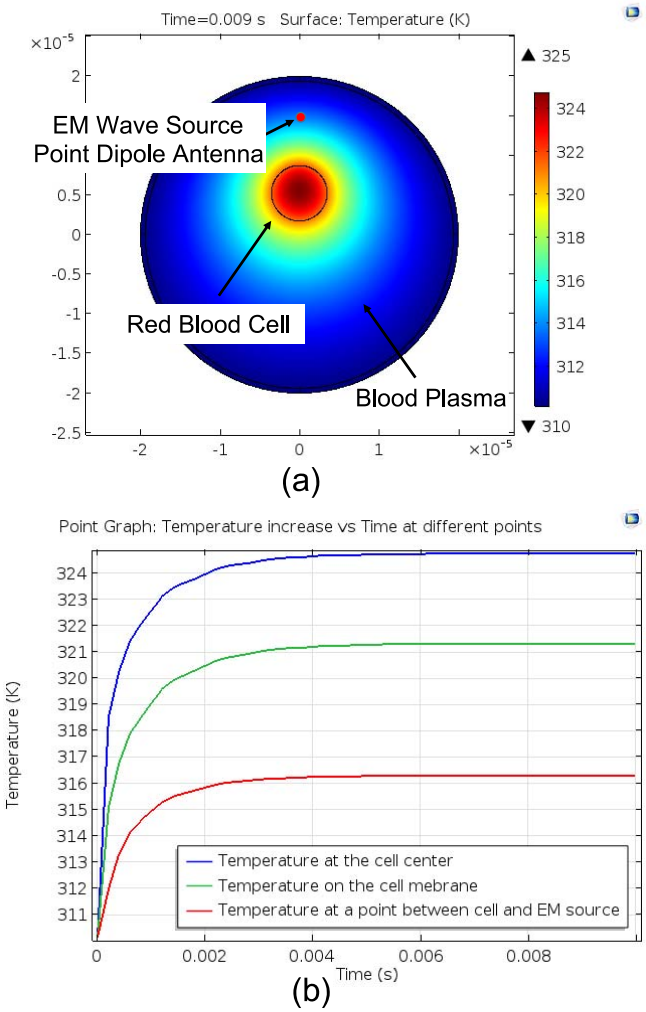

Fig. 4. (a) Heat generation and temperature increase in cells at the presence of EM wave source. (b) Temperature increase vs. time at three different points: at the cell center, on the cell membrane, and between the cell and antenna.

In OOK, the presence of a carrier for a specific duration represents a binary "1", while its absence for the same duration represents a binary "0". Some more sophisticated

schemes vary these durations to convey additional information or prevent errors to happen. For the basic OOK, we consider a carrier signal that is modulated by a Raised Cosine Pulse (RCP-OOK) given by

$$\mathcal{P}_{RCP}(t) = \begin{cases} E_0, & |t| \leq \frac{1-\beta}{2\mathcal{T}_s} \\ \frac{E_0}{2}\left[1+\cos\left(\frac{\pi\mathcal{T}_s}{\beta}\left[|t|-\frac{1-\beta}{2\mathcal{T}_s}\right]\right)\right], & \frac{1-\beta}{2\mathcal{T}_s} < |t| \leq \frac{1+\beta}{2\mathcal{T}_s} \\ 0, & \text{otherwise.}, \end{cases} \tag{11}$$

$\mathcal{T}_s$ is the duration of the pulse or equivalently symbol time, and β is the roll-off factor of the RCP. In order to transmit a "1" by using the RCP-OOK method, the EM source is radiating in the whole period of the symbol time $\mathcal{T}_s$. Depending on the transmission power P_{tx} and the exposure time, the temperature of the exposed biological tissue will increase due to internal molecular vibrations, as discussed in Section III-A. Consequently, to maintain the temperature below a threshold, we must either decrease the power or use shorter pulses. However, neither of these approaches is easily feasible. On the one hand, due to the path loss and noise in the channel, there is a minimum power demand to satisfy the Signal-to-Noise Ratio (SNR) requirements. On the other hand, shortening the symbol time $\mathcal{T}_s$ may lead to missed detections due to the fading phenomenon caused by the cell movements.

In light of these results, we propose, for the first time, the adaptive Gaussian Pulse Train - On-Off Keying modulation (GPT-OOK). The unique advantages of the proposed GPT-OOK modulation technique are twofold: i) power requirements can be met by transmitting shorter pulses, decreasing power consumption, and consequently increasing the maximum available power $P_{\max}$ (see Section III-D), and ii) overcoming possible fading by increasing the number of redundant transmitted pulses in a single symbol, thereby reducing the probability of miss detection.

In GPT-OOK, we modulate the carrier signal with a train of very short Gaussian pulses as follows

$$\mathcal{P}_{GPT}(t) = \frac{E_0}{\sqrt{2\pi}\mathcal{T}_p} e^{-\frac{t^2}{2\mathcal{T}_p^2}}, \tag{12}$$

where $\mathcal{T}_p$ is the Gaussian pulse width. In this method, a train of pulses (spread in time with $\mathcal{T}_d$ delay) is sent to transmit a "1". This provides a redundancy of $\mathcal{N}^R$ given by

$$\mathcal{N}^R = \left\lfloor \frac{\mathcal{T}_s}{\mathcal{T}_d} \right\rfloor. \tag{13}$$

Therefore, the modulated pulse transmits a "1" using either the RCP- or GPT-OOK methods as follows

$$pulse(t) = \begin{cases} \mathcal{P}_{RCP}(t)\cos(2\pi f t), & \text{RCP-OOK is used} \\ \overline{\mathcal{P}_{GPT}(t)}^{\mathcal{N}_R,\mathcal{T}_d}\cos(2\pi f t), & \text{GPT-OOK is used,} \end{cases} \tag{14}$$

where we use the notation $\overline{\mathcal{P}}^{\mathcal{N}_R,\mathcal{T}_d}$ which means that the pulse $\mathcal{P}$ is repeated $\mathcal{N}_R$ times with delay $\mathcal{T}_d$ between the pulse repetitions. Fig. 5 shows (from top to bottom) the digital data stream, modulating pulse and modulated signal with the carrier for (a) RCP and (b) GPT methods. Contrary to RCP, to transmit a "1" by using GPT, the EM source is radiating only in short periods of $\mathcal{T}_p$ with long delays of $\mathcal{T}_d$ in between which prevents excessive temperature increase due to long exposures and allows the biological tissue to cool down between pulses.

C. Random Positioning and Movements of the Cells: Coherence Time of the Channel

The inverse relationship between blood velocity and cross-sectional area is a fundamental principle of fluid dynamics known as the continuity equation and mathematically expressed using

$$A_1 \cdot v_{blood_1} = A_2 \cdot v_{blood_2},$$

where A_1 and A_2 are the cross-sectional areas of two different points along the flow pathway (e.g., two different sections of a blood vessel), v_{blood_1} and v_{blood_2} are the velocities of blood flow at those respective points. This equation states that the product of the cross-sectional area and velocity at any given point along the flow pathway is constant. As the cross-sectional area increases (e.g., from larger arteries to smaller arterioles and capillaries), the velocity of blood flow must decrease to maintain the constant flow rate. Conversely, when the cross-sectional area decreases, the velocity of blood flow increases to compensate and maintain the constant flow rate.

The blood flow velocity is the fastest in the middle of the vessel and slowest at the vessel wall. The fastest speed is in the aorta which is around 40 cm/s, and the slowest is in the capillaries which is close to 0.03 cm/s [39], [40]. These movements cause changes in the properties of the communication channel. Therefore, we define the coherence time of the channel, τ_c, as

$$\tau_c \ll \frac{\lambda_g}{v} = \frac{c}{nfv}, \tag{15}$$

where v is the average speed of cell movements. Further, we define the message time, $\mathcal{T}_{msg}$, which includes the transmission of the required number of bits in a message, N_{bits}, within τ_c as

$$\mathcal{T}_{msg} = N_{bits}\mathcal{T}_s \leq \tau_c \;\Rightarrow\; \mathcal{T}_s \ll \frac{c}{N_{bits}nfv}. \tag{16}$$

The definition of τ_c in (15) and the constraint on the symbol time $\mathcal{T}_s$ given in (16) ensure that the channel properties will not change within the time period of a single message transmission, akin to the slow fading phenomenon. Here, we consider that the channel state information is updated once in every message transmission.

In the specific case of cell movements in the blood, the velocity of the blood v_{blood} can be considered as the speed at which the blood cells move. This speed only applies to the scenario in which the transmitter is fixed (smart band in Fig. 1(a)). However, when the nanomachines are moving along with the cells (Fig. 1(b)) and at the same speed of the blood cells, a much slower relative speed for the cell movements should be considered. In this scenario, the nanomachines effectively "ride along" with the flow of the blood without experiencing significant displacement relative to the cells. As a result, from an external observer's perspective, the apparent

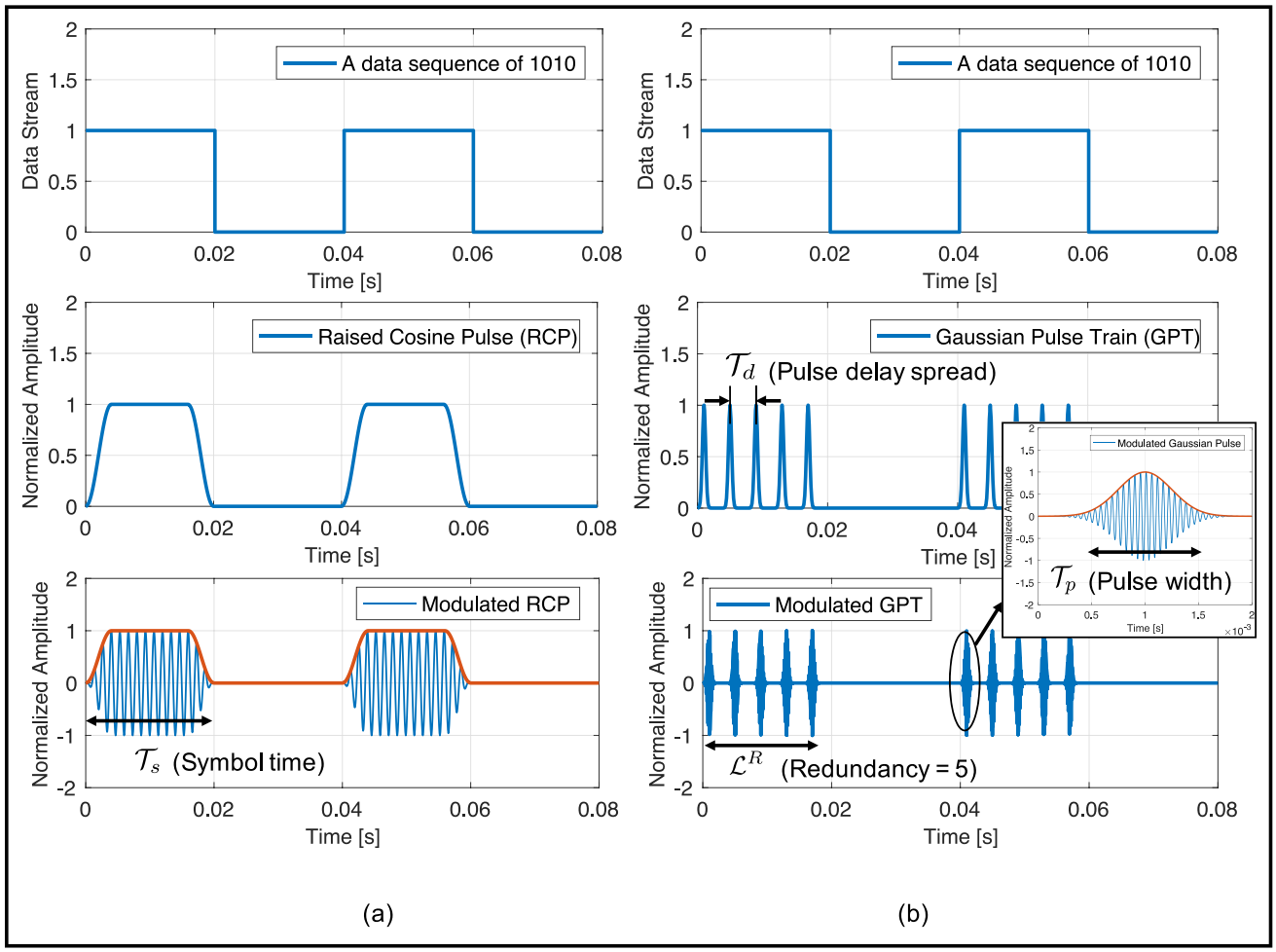

Fig. 5. From top to bottom: Digital data stream, modulating pulse and modulated signal with carrier for (a) RCP and (b) GPT modulation methods.

motion of the cells appears slower compared to when the nanomachines are stationary or moving independently. This results in a larger coherence time τ_c which relaxes the constraint in (16). The same applies to the skin cells, as they are relatively fixed from the wearable device perspective.

D. Power Budget and Noise Model

1) Power Budget: Here we consider the case that the nanomachine is always able to work with the maximum available power which can be calculated from the total available energy $\mathcal{E}_{max}$ in (3). This assumption is true as long as the required data rate does not exceed a threshold which restricts the time needed for the nanogenerator to be able to harvest the maximum possible energy [25] and can be written as follows

$$\mathcal{E}_{max} \leq \lambda_{harv} \mathcal{T}_s, \tag{17}$$

where λ_{harv} is the rate at which the nanogenerator is able to harvest energy in J/s. We further consider that the probability to transmit a logical "0" or a logical "1" in a message of length N_{bits} follows a binary equiprobable distribution ($Pr\{x_0\} = Pr\{x_1\} = 0.5$). Therefore, by using the OOK modulation (as seen in Section III-B), the maximum available power is given as follows

$$P_{max} = \begin{cases} \frac{\mathcal{E}_{max}}{\ddot{\mu}\mathcal{T}_s}, & \text{RCP-OOK is used} \\ \frac{\mathcal{E}_{max}}{\ddot{\mu}\mathcal{N}^R\mathcal{T}_p}, & \text{GPT-OOK is used}. \end{cases} \tag{18}$$

Here $\ddot{\mu} \geq 1$ is the average number of consecutive "1s" (N_{x_1}) received after receiving a "0" and N_{x_1} follows a modified Poisson distribution given as follows

$$Pr\{N_{x_1} = k \mid x_0 \rightarrow x_1\} = e^{-\ddot{\mu}} \frac{\ddot{\mu}^{k-1}}{(k-1)!}, \quad \forall k \geq 1, \tag{19}$$

where k is an integer bigger than one and $x_0 \rightarrow x_1$ represent a transition of "0" to "1" in the received sequence of bits. Note that we assume that the nanogenerator is able to harvest energy only during the silence time. However, in the GPT-OOK modulation mode if the delay between the pulses is much bigger than the pulse width ($\mathcal{T}_d \gg \mathcal{T}_p$), then the nanogenerator is able to store some energy in between the pulses, hence the maximum available power can be increased up to $\mathcal{E}_{max}/\mathcal{T}_p$. Moreover, we consider that the available power in the smart band is always more than that of the nanomachine (due to the larger battery that can be placed in a wearable device) and it does not introduce a predominant constraint on P_{max}.

2) Noise Model: Noise in a sensing system can corrupt the detected signals and significantly affect the sensing capability. In the intra-body communication system shown in Fig. 1, two primary noises can be considered, namely, the channel noise and the device noise. Therefore, the total noise temperature of the system is given as

$$T_{sys} = T_{channel} + T_{device}. \tag{20}$$

The channel noise, $T_{channel}$, is mainly caused by the molecular absorption discussed in Section III-A, which not only generates heat and affects the properties of the channel in terms of attenuation, but also introduces noise [41], [42]. The equivalent noise temperature due to the molecular absorption that an omnidirectional antenna receives from the medium is given as

$$T_{mol}(f, d) = T_0 \varepsilon(f, d), \tag{21}$$

where T_0 is the reference temperature of the medium and ε refers to the emissivity of the channel which is defined as $\varepsilon(f, d) = 1 - \zeta(f, d)$ where ζ is the transmissivity of the medium and is obtained by using the Beer-Lambert law as

$$\zeta(f, d) = \frac{P_0}{P_i} = e^{-\bar{\alpha}(f)d}, \tag{22}$$

where P_i and P_0 are the incident and radiated powers and $\bar{\alpha}$ is the medium absorption coefficient.

The device noise is mainly defined by the antenna noise temperature, T_{ant}, which describes how much noise a receiver antenna produces in a given environment. This noise depends on the frequency of the EM wave and for the specific case of optical wave radiations it is considered as Shot noise (Poisson noise) due to the discrete nature of the photon detectors (photon counters) at the receiver device. In any case, the calculation of the device noise is out of the scope of the current study. We consider the receiver antenna to have a very low noise temperature compared to the channel noise temperature.

The dominant noise temperature of the system T_{sys} is the channel noise which is caused by the molecular absorption T_{mol}. The equivalent molecular absorption noise power at the receiver, for a given bandwidth *B*, can be calculated as

$$P_n(f, d) = \int_B \mathcal{N}(f, d) df = k_B \int_B T_{mol}(f, d) df, \tag{23}$$

where $\mathcal{N}$ refers to the noise power spectral density, k_B is the Boltzmann constant and T_{mol} refers to the equivalent molecular absorption noise temperature given by (21).

IV. Optimization Problem Formulation and Solution

In this section, we formulate an optimization problem for EM intra-body communications with the objective of minimizing the temperature increase in biological tissues while maintaining a minimum QoS requirement. This will be achievable by using our proposed modulation technique, GPT-OOK, given in Section III.

A. Formulating the Optimization Problem

As discussed in Section III-A and based on (10), the temperature increases exponentially while the radiation source is "ON". The total temperature increase T_{inc} after a successful transmission of a logical "1" by using the GPT-OOK modulation method with $\mathcal{N}^R$ redundant pulses within a symbol is

$$\begin{aligned} T_{inc} &= \Theta\left(\mathcal{T}_p, \mathcal{T}_d, \mathcal{N}^R\right) \\ &= \Delta T_{max}\left(1 - e^{-\frac{\mathcal{T}_p}{\mathcal{T}_{inc}}}\right) \sum_{i=1}^{\mathcal{N}^R} \left[\left(1 - e^{-\frac{\mathcal{T}_p}{\mathcal{T}_{inc}}}\right) e^{-\frac{\mathcal{T}_d}{\mathcal{T}_{dec}}}\right]^{i-1}. \end{aligned} \tag{24}$$

Note that we estimate the Gaussian pulse with a sharp rectangular shape which means that as soon as the radiation source is "ON" it starts to radiate with the maximum power. It can be seen from (24) that T_{inc} depends on pulse width $\mathcal{T}_p$, delay $\mathcal{T}_d$, and number of redundant pulses in a symbol $\mathcal{N}^R$, which are the main parameters of the GPT-OOK modulation scheme.

We consider the BER as the QoS measure. The maximum tolerable BER, BER_{max}, is defined as a requirement that guarantees the successful transmission of a message of length N_{bits} within τ_c. This is defined as the minimum achievable throughput of the system $\mathcal{S}_{min}$ given as $\mathcal{S}_{min} = N_{bits}/\tau_c$. The BER is a function of the path loss $\mathcal{L}(d)$, SNR, $\mathcal{N}^R$, $\mathcal{T}_p$, and pulse probability p_x. The larger the SNR, $\mathcal{N}^R$ and $\mathcal{T}_p$, the smaller the path loss $\mathcal{L}(d)$, resulting in a better BER. The SNR$= \mathcal{E}_{tx}^{bit}/P_n$, where $\mathcal{E}_{tx}^{bit}$ is the energy required to transmit a bit and P_n is the noise power given in (23).

Minimizing the temperature increase by using the proposed GPT-OOK modulation technique and by taking into consideration the device, channel and biocompatibility constraints can be given in the form of an optimization problem as follows

Optimization Problem [P1]

$$\begin{aligned} &Given: \tau_c, \mathcal{T}_{inc}, \mathcal{T}_{dec}, \ddot{\mu}, f, P_n, \mathcal{E}_{max}, \mathcal{S}_{min}, \\ &B_{max}, BER_{min}, \mathcal{N}_{min}^R, T_0, T_{thr}, \Delta T_{max} \\ &Find: \mathcal{T}_p^*, \mathcal{T}_d^*, \mathcal{N}^{R*} \\ &Minimize: T_{inc} = \Theta\left(\mathcal{T}_p, \mathcal{T}_d, \mathcal{N}^R\right) \\ &Subject\ to: \\ &\mathcal{T}_p \geq \frac{1}{B_{max}} && (25) \\ &\mathcal{T}_d \leq \frac{\mathcal{T}_s}{\mathcal{N}_{min}^R} && (26) \\ &\mathcal{T}_s \leq \frac{N_{bit}}{\mathcal{S}_{min}} && (27) \\ &\mathcal{T}_s \ll \frac{c}{N_{bits} nfv} && (28) \\ &\mathcal{E}_{max} \leq \lambda_{harv} \mathcal{T}_s, && (29) \\ &P_{max} = \frac{\mathcal{E}_{max}}{\ddot{\mu} \mathcal{N}^R \mathcal{T}_p} && (30) \\ &\phi\left(\frac{\mathcal{L}(d) P_n}{\mathcal{E}_{tx}^{bit} \mathcal{N}^R \mathcal{T}_p}, p_x\right) \leq BER_{max} && (31) \\ &T_{inc} \leq T_{thr} - T_0. && (32) \end{aligned}$$

In **[P1]**, B_{max} is the maximum available bandwidth, ϕ is a function that gives the BER and $\mathcal{N}^R_{min}$ is the minimum required redundant pulses to satisfy the BER constraint in (31). Constraints (25) to (28) relate to the modulation technique parameters. The device and communication interdependencies are given by (29) and (30). Inequality (31) in parallel with (27) and (28) satisfies the minimum QoS requirement. Finally, (32) guarantees the biocompatibility of the proposed modulation technique for EM intra-body communications.

It can be observed that the problem defined in **[P1]** is a joint variable optimization problem with variables $\mathcal{T}_p$, $\mathcal{T}_d$ and $\mathcal{N}^R$, and a mixture of linear and non-linear constraints on the optimization variables given as both equalities and inequalities. Seeking optimal solutions with traditional multi-objective optimization methods for problems involving the coupling of multiple optimization problems that are competing in nature and yet must simultaneously satisfy various conflicting objectives is very difficult, if not impossible, particularly in the specific case of nanomachines with restricted computational capabilities.

Solving these so-called "joint optimization problems" usually requires game theory approaches to achieve equilibrium solutions that leverage multiple conflicting goals of design. In addition, for the specific case of **[P1]**, proving the convexity of the objective function and the constraint set is not trivial. However, it can be shown that the objective function Θ is convex with respect to the variable $\mathcal{T}_p$, and furthermore, the constraints can be approximated with convex sets. In the following section, we propose a solution to **[P1]** and numerically study the achievable results.

B. Optimization Problem Solution Approach

It is to be noted that in our system we consider a desired bitrate of 100kbps, which is the main parameter that directly affects the symbol rate and hence the T_d (depending on the required N_r to satisfy a desired BER). The T_p is impacted by the B_{max} which is in the GHz range, i.e., T_p can be as small as few ns/ms, therefore it is practical to assume $T_p \ll T_d$. Thereby, T_{inc} can be approximated as:

$$T_{inc} = \Theta\left(\mathcal{T}_p, \mathcal{T}_d, \mathcal{N}^R\right) \approx \Delta T_{max}\left(1 - e^{-\frac{\mathcal{T}_p}{\mathcal{T}_{inc}}}\right). \quad (33)$$

Here, we consider a restricted version of GPT-OOK in which $\mathcal{T}_d = n\mathcal{T}_p$ with *n* being a sufficiently large integer that satisfies the approximation in (33). It can be observed that the new objective function $\Theta^{\mathcal{M}}$ (right hand side of (33)) is a convex function with only one optimization variable $\mathcal{T}_p$.

Regarding the constraints of the problem **[P1]**, we assume the total number of required bits in a message N_{bits} is fixed and given. Therefore, inequality constraints (27) and (28) will be reduced to $\mathcal{T}_s = \tau_c / N_{bits}$ and inequality (29) will be reduced to $\mathcal{E}_{max} = \lambda_{harv}\mathcal{T}_s$. Both of the new equality constraints now can be considered as a given initial value of the optimization problem. Moreover, the constraints on the maximum available energy due to energy harvesting process and the communications requirements given by (29) and (30) can be considered to be always restricted by the nanolaser antenna propagation capability (i.e., $P^{nanolaser}_{max} < P^{available}_{max}$); hence, P_{max} can be assumed to be given by the nanolaser antenna as an initial value and is not affected by the optimization variable $\mathcal{T}_p$.

TABLE I
SIMULATION AND NUMERICAL ANALYSIS PARAMETERS AND CONSTANTS

Symbol	Quantity	Valus [Units]
T_0	Normal body temperature	310.15 [°K]
T_{thr}	Tolerable temperature threshold	316.15 [°K]
CEM_{43}	Cumulative equivalent minutes at 43 °C	[min]
$\mathcal{C}$	Specific heat capacity of human blood	4.45e3 [J/kg°K]
ρ	Density of human blood	1060 [kg/m^3]
k	Thermal conductivity of human blood	0.53 [W/m.K]
r_{cell}	Radius of red blood cell	[3.5 µm]
ϵ_r	Relative permittivity of red blood cell	2.0406+j0.0034
μ_r	Relative permeability of red blood cell	1
p	Electric current dipole moment	5.7e-3 [A.m]
$\mathcal{T}_p$	Pulse width in GPT-OOK modulation	[s]
$\mathcal{T}_d$	Pulse delay in a GPT-OOK symbol	$10\mathcal{T}_p$ [s]
$\mathcal{T}_{inc}$	Temperature increase time constant	1 [ms]
$\mathcal{T}_{dec}$	Temperature decrease time constant	4 [ms]
λ	Wavelength	600 [nm]
B_{max}	Maximum available bandwidth	0.001 [THz]
BER_{min}	Minimum required BER	1e-2

Finally, under the aforementioned assumption of $\mathcal{T}_d = n\mathcal{T}_p$, inequality (26) can be replaced by $\mathcal{T}_p \leq \mathcal{T}^{max}_p$. We can also merge (25) and (31) into one inequality given as $\mathcal{T}^{min}_p \leq \mathcal{T}_p$. In addition, we consider a Return to Zero (RTZ) coding technique in our communication system. The benefits of using the RTZ coding are twofold: i) there is no need to have a separate clock for synchronization in the system, and ii) the tissue temperature always has enough time to cool down before the next pulse comes in, and it also simplifies (18) by setting $\ddot{\mu} = 1$. With the new objective function and modified constraints the equivalent optimization problem can be written as

Optimization Problem [P2]

$$\begin{aligned}
&Given: \tau_c, \mathcal{T}_{inc}, \mathcal{T}_{dec}, \ddot{\mu}, f, P_n, \mathcal{E}_{max}, \mathcal{S}_{min},\\
&B_{max}, BER_{min}, \mathcal{N}^R_{min}, T_0, T_{thr}, \Delta T_{max}, n\\
&Find: \mathcal{T}^*_p\\
&Minimize: T_{inc} = \Theta^{\mathcal{M}}(\mathcal{T}_p)\\
&Subject\ to:\\
&\quad \mathcal{T}^{min}_p \leq \mathcal{T}_p \leq \mathcal{T}^{max}_p \quad (34)\\
&\quad T_{inc} \leq T_{thr} - T_0 \quad (35)
\end{aligned}$$

It can be easily observed that **[P2]** is a convex optimization problem. Moreover, the objective function is monotonically increasing on the feasible set. Therefore the optimal solution of **[P2]** is given as $\mathcal{T}^*_p = \mathcal{T}^{min}_p$.

Note that the assumption of fixed N_{bits} may cause the feasible set for the system of inequalities in **[P2]** to become an empty set (i.e., $\tau^{max}_p < \tau^{min}_p$ or $\Theta^{\mathcal{M}}(\mathcal{T}^{min}_p) \geq T_{thr} - T_0$). In this case we have to reduce the message size and solve the optimization problem again to obtain a feasible optimal solution. To avoid this, the maximum message size that satisfies the temperature threshold can be further calculated and be considered as the initial input of the problem.

V. Numerical Analysis

We use OOK modulation, in which the presence of a signal is represented by transmitting a carrier wave with a specific amplitude, while the absence of a signal is represented by transmitting no carrier wave (i.e., turning it off). This binary modulation scheme can be interpreted as Binary Amplitude Shift Keying (BASK), where the amplitude of the carrier wave varies to represent binary data. In both cases, there are two possible states: one where the carrier wave is present (with a certain amplitude) representing one binary state (in our case "1"), and another where the carrier wave is absent (with zero amplitude) representing the other binary state (in our case "0").

ASK and OOK communication protocols are commonly employed in short-range wireless applications, allowing power savings as no signal is transmitted during 0's (half of the time). On the receiver side, we utilize a non-coherent detector, easily implemented with a low-cost envelope detector. This detector is convenient for nanomachines as it employs simple passive components and doesn't necessitate a reference or carrier signal. In addition, we implement OOK in two modes: the first mode involves a simple OOK using a RCP as the modulating pulse as depicted in Fig. 5 with RCP-OOK. The second mode employs our proposed train of short Gaussian pulses, shown with GPT-OOK in Fig. 5. For completeness, we also evaluate Single Short Pulse (SSP) transmission, where only one pulse with the same duration as GPT pulses is transmitted without redundancy. While SSP offers the advantage of minimal heat generation, as demonstrated later, it suffers from a significantly high BER.

Table I summarizes the parameters and constants that we use for the numerical analysis of the proposed modulation technique for iWNSNs. The wavelength of the EM wave is considered 600 nm for a visual optical signal in free space (which is equivalent to 450 nm in blood considering a refractive index of 1.33). Hence the frequency of the modulator signal is 500 THz. Fig. 6(a) shows the COMSOL simulation of moving RBCs in a human blood vessel with a pair of transmitting and receiving nanosensors, while Fig. 6(b) illustrates the snapshot of the received signal at 20 time steps each 5 μs apart [43]. To simulate the movements of RBCs in a blood vessel using COMSOL, we first randomly place a number of cells with predefined radii inside a section of a vessel containing two nanomachines. Then, employing a random motion algorithm, we determine the new position of each cell at each step using the Wiener process. In the context of Brownian motion, the random movement of RBCs in the propagation medium create variations in the signal's path length and phase, leading to constructive and destructive interference at the receiver. This results in the signal experiencing random fluctuations in amplitude, which is characteristic of Rayleigh fading. In fact, the movement of cells in a complex biological environment involves unpredictable trajectories, collisions, and interactions, contributing to a stochastic nature akin to the random phase variations in Rayleigh fading.

It is worth mentioning that we only consider RBCs inside the human blood, as RBCs are the largest (7 microns) and most abundant (45%), thus exerting the greatest influence on

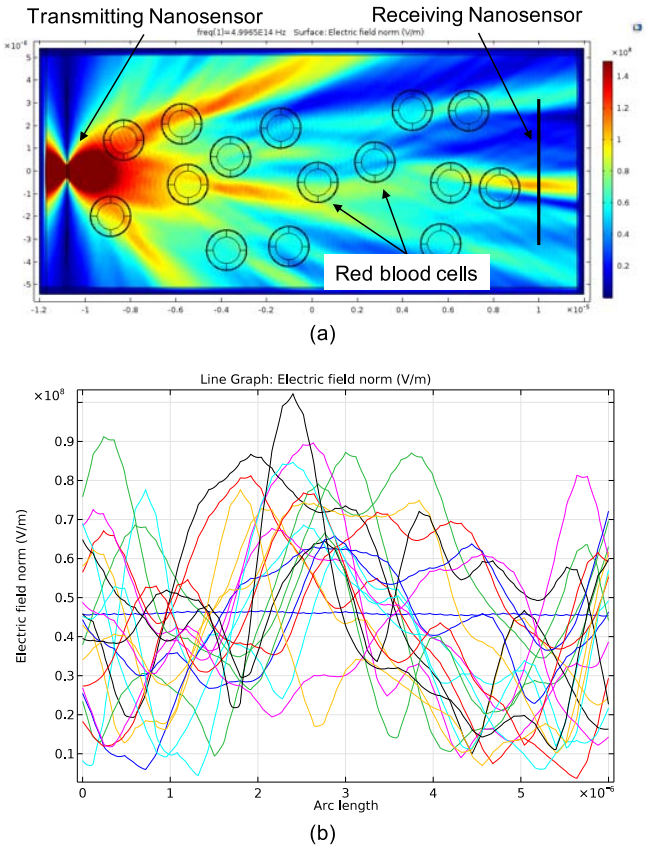

Fig. 6. (a) Moving RBCs inside a human blood vessel. (b) Received signal at the receiver node.

light propagation in blood. All blood cells float within blood plasma, which constitutes 55% of blood and is primarily (92%) composed of water. In addition, platelets and some types of white blood cells, may appear relatively transparent compared to RBCs. These cells are generally less pigmented and have fewer cellular components compared to RBCs. As a result, they exhibit less light absorption and appear less opaque when viewed under a microscope or in microscopic imaging.

To evaluate the performance of our proposed modulation technique, GPT-OOK, against the RCP-OOK, we use a Rayleigh fading model with a maximum Doppler shift calculated using $f_D^{max} = \frac{v}{c/n} f$. The cell movements speed ranges between 0.004 m/s to 0.4 m/s inspired from the motion of the blood cells. By substituting the cell speed in the Doppler shift formula, the derived maximum shift will range approximately between 9 kHz and 900 kHz. Note that in OOK, every symbol represents one bit, so bit/sec and symbol/sec are equivalent. We consider a 90 kbit/s transmission rate to evaluate the BER for the entire range of the Doppler applicable to both the minimum and maximum speeds of the cells. Fig. 7 shows a random sequence of bits transmitted (top) and received (bottom) in an intra-body communication channel. The red line shows the cell movements and cell blocking effect that is modeled with a Rayleigh fading model with Doppler of 9 kHz.

Fig. 8 shows the BER of different modulation techniques, namely, RCP which uses a long pulse to transmit a "1" and

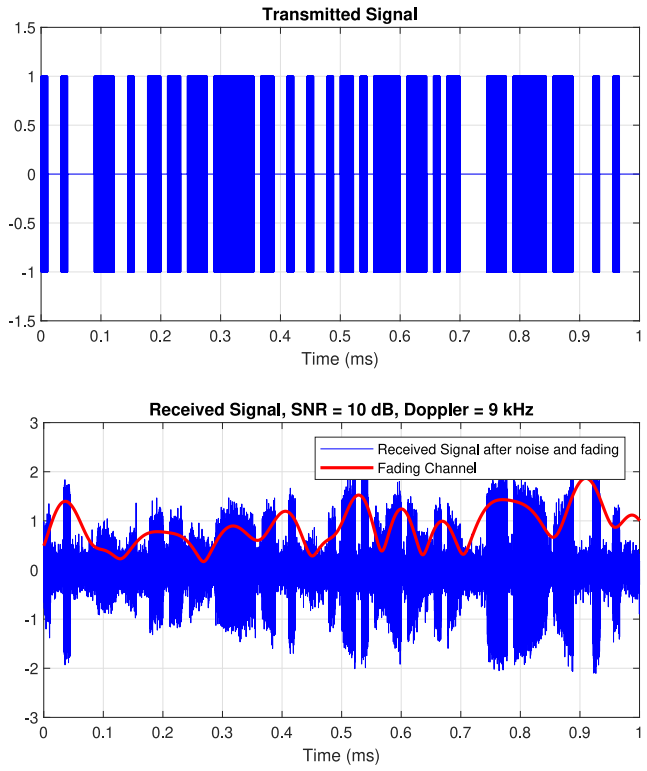

Fig. 7. Random sequence of bits transmitted (top) and received (bottom) in an intra-body communication channel with noise and fading. Cell blocking effect is modeled with a Rayleigh fading model with Doppler of 9 kHz.

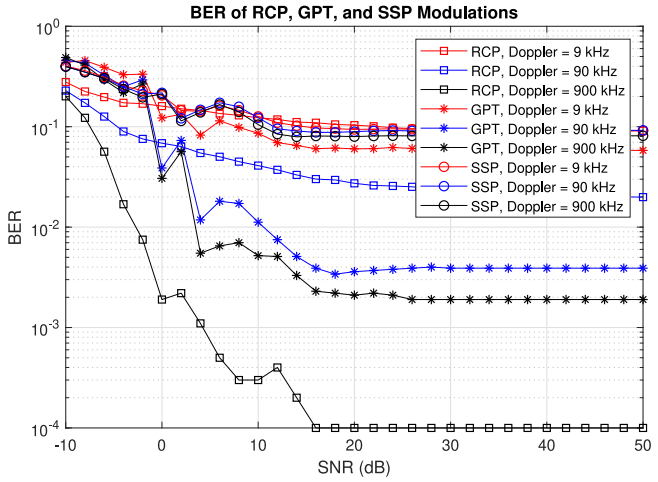

Fig. 8. BER of RCP, GPT and SSP vs. SNR at different cell movement speeds modeled by a Rayleigh channel with various Doppler shifts.

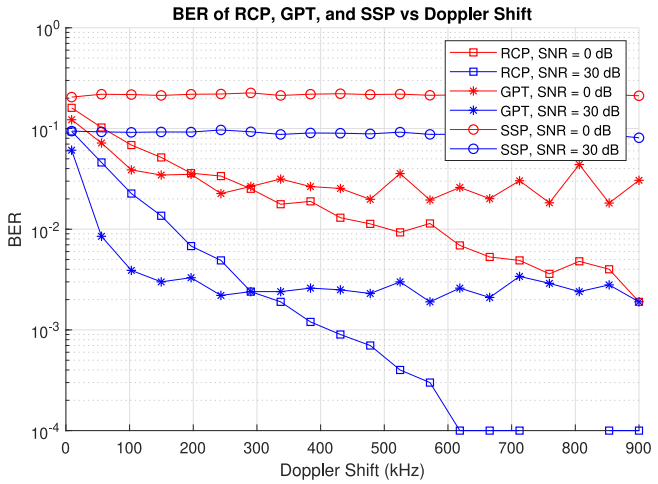

Fig. 9. BER of RCP, GPT and SSP vs Doppler shift.

silence for a "0"; GPT which uses a train of redundant short pulses with $\mathcal{N}^R = 5$ and $\mathcal{T}_p = 0.1\mathcal{T}_d$; and SSP which uses only one short pulse (no redundancy) with same duration of $\mathcal{T}_p$ in GPT. The results are shown for a range of Doppler shifts from 9 kHz to 900 kHz. As it can be seen in Fig. 8, our proposed modulation technique, GPT, can easily achieve BER of less than 10^{-2} for Doppler shifts larger than 90 kHz. This translates to cell movement speeds of 0.04 m/s and 0.4 m/s which is the average speed of RBCs in the center of blood vessels. The speed of cells decreases near the vessel walls with a minimum of ∼0.004 m/s which is modeled by a 9 kHz Doppler effect showing a high BER ($\sim 10^{-1}$). Note that slow cell movements can block the signal for a longer duration, hence even the RCP cannot achieve a good BER. However, this only occurs when the sensors are in close proximity to the vessel wall, which has a very low probability. Nevertheless, a longer pulse duration can serve as a remedy for this specific case, albeit at the expense of a lower data rate.

From Fig. 8, it can also be observed that SSP cannot achieve a good BER. Due to the use of very short pulses and a longer delay between two consecutive pulses, SSP causes the lowest temperature increase among other techniques. However, it suffers from poor communication quality. RCP achieves the best BER at a Doppler of 900 kHz, and GPT can easily meet the minimum BER requirement of 10^{-2}.

Fig. 9 shows the BER for different speeds of cells. It can be seen that GPT performs even better than RCP when the speed of cells is comparable to the bit rate, i.e., 90 kbit/s at 0.04 m/s (90 kHz Doppler). Therefore, GPT is the optimal technique which preserves the communication quality while preventing long-duration EM exposure of the biological tissues, causing lower temperature increase.

In an extreme case where the pulse "ON" time needs to be longer (e.g., low SNR, poor channel condition, or slower cell movements), it can be shown that GPT still works better than RCP while keeping the temperature increase below the safety threshold. Fig. 10 shows the temperature increase using RCP- and GPT-OOK modulation techniques with a pulse duration of 20 ms. As it can be seen in Fig. 10, the temperature goes above the tolerable threshold T_{thr} when using the RCP-OOK with a rather large "ON" time. However, by using the GPT-OOK (with the same power), the temperature remains below the threshold T_{thr}. This is due to the fact that in GPT, each pulse duration in the pulse train is very short which only causes a small temperature increase. Then, between the short pulses and before the next pulse, the tissue's temperature decreases; hence, the overall temperature increase will always remain below the safety threshold.

Finally, Fig. 11 shows temperature increase T_{inc} in biological tissues in the presence of the EM intra-body communication by using RCP- and GPT-OOK modulation techniques vs. the achievable throughput $\mathcal{S}_{min}$. It is worth mentioning that we only account for the temperature increase

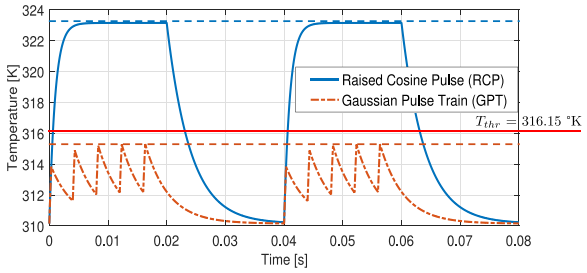

Fig. 10. Temperature increase and decrease in biological tissues in presence of the EM wave vs time.

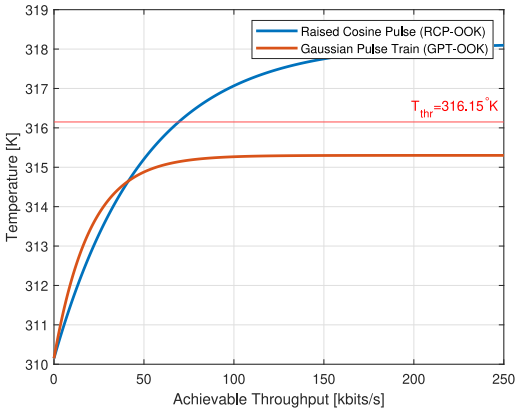

Fig. 11. Temperature increase T_{inc} in biological tissues in the presence of the EM intra-body communication by using RCP- and GPT-OOK modulation techniques vs achievable throughput $\mathcal{S}_{min}$.

in the nearest cell to the transmission source as the worst-case scenario in temperature increase. Note that the other cells will absorb less energy due to their longer distance from the source, resulting in a lower temperature increase. As seen in Fig. 11, the heat generated in the biological tissues can always be maintained below the safety threshold T_{thr} by using the proposed GPT-OOK method, even for higher throughputs. It can also be observed that RCP-OOK generates less heat compared to GPT-OOK for very small ranges of throughput. This is due to the fact that RCP pulses have a smoother transition between symbols compared to GPT, resulting in better bandwidth efficiency. However, even with a slight increase in throughput demand, the heat generated by RCP exceeds that of the GPT method and eventually surpasses the safety threshold.

VI. Conclusion

In this paper, we propose a biocompatible modulation technique for iWNSNs. Specifically, we develop a mathematical framework to optimize the parameters of an adaptive Time Spread OOK pulse-based modulation named GPT-OOK. This optimization considers the physics of the intra-body optical channel and the light-matter interaction in biological tissues, accounting for the resulting photo-thermal effects.

Moreover, we formulate and solve an optimization problem to minimize the biological impact of EM waves while meeting the minimum QoS requirements for intra-body communications. The proposed modulation technique and the analytical optimization model are validated through extensive numerical simulations. The presented results indicate a trade-off between the link efficiency and the biocompatibility of transmitted signals, with optimal modulation parameters preventing potential harmful effects to biological tissues based on the photosensitivity of target regions.

Numerical analysis demonstrates that GPT-OOK achieves a data rate of 90 kbit/s BER of 10^{-2} while keeping the temperature increase within the bio-safety measures. This indicates a reliable intra-body channel facilitating data transmission without significant loss or corruption.

As a future research direction, investigating methods for dynamic adaptation of modulation parameters based on real-time feedback from the intra-body environment could further enhance the performance and biocompatibility of wireless intra-body communication. In addition, exploring the integration of multiple communication modalities, such as optical, acoustic, and EM could offer synergistic benefits for intra-body wireless communications. By leveraging the strengths of each modality, the communication system can adapt to variations in tissue properties, maximizing signal penetration and minimizing signal loss.

References

[1] Y. Fu and Q. Ma, "Recent developments in electrochemiluminescence nanosensors for cancer diagnosis applications," *Nanoscale*, vol. 12, no. 26, pp. 13879–13898, 2020.
[2] G. Lee and J. A. Rogers, "Molecular engineering of nanoactuators for neuromodulation," *Matter*, vol. 5, no. 6, pp. 1631–1633, 2022.
[3] S. Wirdatmadja et al., "Analysis of light propagation on physiological properties of neurons for nanoscale optogenetics," *IEEE Trans. Neural Syst. Rehabil. Eng.*, vol. 27, no. 2, pp. 108–117, Feb. 2019.
[4] J.-R. Choi et al., "Implantable neural probes for brain-machine interfaces–current developments and future prospects," *Exp. Neurobiol.*, vol. 27, no. 6, p. 453, 2018.
[5] C. L. Wong and M. Olivo, "Surface plasmon resonance imaging sensors: A review," *Plasmonics*, vol. 9, no. 4, pp. 809–824, 2014.
[6] H. H. Nguyen, J. Park, S. Kang, and M. Kim, "Surface plasmon resonance: A versatile technique for biosensor applications," *Sensors*, vol. 15, no. 5, pp. 10481–10510, 2015.
[7] M. Vendrell, K. K. Maiti, K. Dhaliwal, and Y.-T. Chang, "Surface-enhanced raman scattering in cancer detection and imaging," *Trends Biotechnol.*, vol. 31, no. 4, pp. 249–257, 2013.
[8] L. Wu and X. Qu, "Cancer biomarker detection: Recent achievements and challenges," *Chem. Soc. Rev.*, vol. 44, no. 10, pp. 2963–2997, 2015.
[9] M. P. Nezhad et al., "Room-temperature subwavelength metallo-dielectric lasers," *Nat. Photon.*, vol. 4, no. 6, pp. 395–399, 2010.
[10] R. F. Oulton et al., "Plasmon lasers at deep subwavelength scale," *Nature*, vol. 461, no. 7264, p. 629, 2009.
[11] J. Dorfmuller, R. Vogelgesang, W. Khunsin, C. Rockstuhl, C. Etrich, and K. Kern, "Plasmonic nanowire antennas: Experiment, simulation, and theory," *Nano Lett.*, vol. 10, no. 9, pp. 3596–3603, 2010.
[12] M. Nafari and J. M. Jornet, "Modeling and performance analysis of metallic plasmonic nano-antennas for wireless optical communication in nanonetworks," *IEEE Access*, vol. 5, pp. 6389–6398, 2017.
[13] L. Tang et al., "Nanometre-scale germanium photodetector enhanced by a near-infrared dipole antenna," *Nat. Photon.*, vol. 2, no. 4, pp. 226–229, 2008.
[14] P. Bai, M.-X. Gu, X.-C. Wei, and E.-P. Li, "Electrical detection of plasmonic waves using an ultra-compact structure via a nanocavity," *Opt. Exp.*, vol. 17, no. 26, pp. 24349–24357, 2009.
[15] H. Guo, P. Johari, J. M. Jornet, and Z. Sun, "Intra-body optical channel modeling for in vivo wireless nanosensor networks," *IEEE Trans. Nanobiosci.*, vol. 15, no. 1, pp. 41–52, Jan. 2016.
[16] P. Johari and J. M. Jornet, "Nanoscale optical wireless channel model for intra-body communications: Geometrical, time, and frequency domain analyses," *IEEE Trans. Commun.*, vol. 66, no. 4, pp. 1579–1593, Apr. 2018.

[17] L. Miccio, P. Memmolo, F. Merola, P. Netti, and P. Ferraro, "Red blood cell as an adaptive optofluidic microlens," *Nat. Commun.*, vol. 6, p. 6502, Mar. 2015.
[18] M. Choi, J. W. Choi, S. Kim, S. Nizamoglu, S. K. Hahn, and S. H. Yun, "Light-guiding hydrogels for cell-based sensing and optogenetic synthesis in vivo," *Nat. Photon.*, vol. 7, no. 12, pp. 987–994, 2013.
[19] H. Elayan, R. M. Shubair, J. M. Jornet, and P. Johari, "Terahertz channel model and link budget analysis for intrabody nanoscale communication," *IEEE Trans. Nanobiosci.*, vol. 16, no. 6, pp. 491–503, Sep. 2017.
[20] H. Elayan, A. W. Eckford, and R. S. Adve, "Information rates of controlled protein interactions using terahertz communication," *IEEE Trans. Nanobiosci.*, vol. 20, no. 1, pp. 9–19, Jan. 2021.
[21] H. H. Richardson, M. T. Carlson, P. J. Tandler, P. Hernandez, and A. O. Govorov, "Experimental and theoretical studies of light-to-heat conversion and collective heating effects in metal nanoparticle solutions," *Nano Lett.*, vol. 9, no. 3, pp. 1139–1146, 2009.
[22] H. Elayan, P. Johari, R. M. Shubair, and J. M. Jornet, "Photothermal modeling and analysis of intrabody terahertz nanoscale communication," *IEEE Trans. Nanobiosci.*, vol. 16, no. 8, pp. 755–763, Dec. 2017.
[23] S. Wu, P. Johari, N. Mastronarde, and J. M. Jornet, "On the photothermal effect of intra-body nano-optical communications on red blood cells," in *Proc. IEEE Conf. Comput. Commun. Workshops (INFOCOM WKSHPS)*, 2018, pp. 645–650.
[24] J. M. Jornet and I. F. Akyildiz, "Joint energy harvesting and communication analysis for perpetual wireless nanosensor networks in the terahertz band," *IEEE Trans. Nanotechnol.*, vol. 11, no. 3, pp. 570–580, May 2012.
[25] P. Johari and J. M. Jornet, "Packet size optimization for wireless nanosensor networks in the terahertz band," in *Proc. IEEE Int. Conf. Commun. (ICC)*, 2016, pp. 1–6.
[26] M. H. Anisi, G. Abdul-Salaam, M. Y. I. Idris, A. W. A. Wahab, and I. Ahmedy, "Energy harvesting and battery power based routing in wireless sensor networks," *Wireless Netw.*, vol. 23, pp. 249–266, Dec. 2017.
[27] M. Pierobon, J. M. Jornet, N. Akkari, S. Almasri, and I. F. Akyildiz, "A routing framework for energy harvesting wireless nanosensor networks in the Terahertz band," *Wireless Netw.*, vol. 20, pp. 1169–1183, Jul. 2014.
[28] S. L. Jacques, "Optical properties of biological tissues: A review," *Phys. Med. Biol.*, vol. 58, no. 11, pp. R37–61, 2013.
[29] S. A. Prahl, M. Keijzer, S. L. Jacques, and A. J. Welch, "A monte carlo model of light propagation in tissue," *Dosim. Laser Radiat. Med. Biol.*, vol. 5, pp. 102–111, Jan. 1989.
[30] L. Wang and S. L. Jacques, *Monte Carlo Modeling of Light Transport in Multi-Layered Tissues in Standard C*, Univ. Texas MD Anderson Cancer Center, Houston, TX, USA, 1992.
[31] J. C. Lin, *Electromagnetic Fields in Biological Systems*. Boca Raton, FL, USA: CRC press, 2011.
[32] P. Johari and J. M. Jornet, "Nanoscale optical channel modeling for in vivo wireless nanosensor networks: A geometrical approach," in *Proc. IEEE Int. Conf. Commun. (ICC)*, 2017, pp. 1–6.
[33] "COMSOL multiphysics simulation software." COMSOL. Accessed: Mar. 2024. [Online]. Available: http://www.comsol.com/products/multiphysics/
[34] D. A. B. Miller, *Quantum Mechanics for Scientists and Engineers*. New York, NY, USA: Cambridge Univ. Press, 2008.
[35] M. W. Dewhirst, B. Viglianti, M. Lora-Michiels, M. Hanson, and P. Hoopes, "Basic principles of thermal dosimetry and thermal thresholds for tissue damage from hyperthermia," *Int. J. Hyperth.*, vol. 19, no. 3, pp. 267–294, 2003.
[36] P. S. Yarmolenko et al., "Thresholds for thermal damage to normal tissues: An update," *Int. J. Hyperth.*, vol. 27, no. 4, pp. 320–343, 2011.
[37] S. A. Sapareto and W. C. Dewey, "Thermal dose determination in cancer therapy," *Int. J. Radiat. Oncol. Biol. Phys.*, vol. 10, no. 6, pp. 787–800, 1984.
[38] R. H. Pletcher, J. C. Tannehill, and D. Anderson, *Computational Fluid Mechanics and Heat Transfer*. Boca Raton, FL, USA: CRC Press, 2012.
[39] G. B. Thurston, "The viscosity and viscoelasticity of blood in small diameter tubes," *Microvasc. Res.*, vol. 11, no. 2, pp. 133–146, 1976.
[40] E. Marieb and K. Hoehn, *Human Anatomy & Physiology*. London, U.K.: Pearson Educ., 2015. [Online]. Available: https://books.google.ca/books?id=ac2gBwAAQBAJ
[41] F. Box, "Utilization of atmospheric transmission losses for interference-resistant communications," *IEEE Trans. Commun.*, vol. 34, no. 10, pp. 1009–1015, Oct. 1986.
[42] J. M. Jornet and I. F. Akyildiz, "Channel modeling and capacity analysis of electromagnetic wireless nanonetworks in the Terahertz band," *IEEE Trans. Wireless Commun.*, vol. 10, no. 10, pp. 3211–3221, Oct. 2011.
[43] P. Johari and J. M. Jornet, "An optofluidic channel model for in vivo nanosensor networks in human blood," in *Proc. SPIE Defense + Secur. Conf., Int. Soc. Opt. Photon.*, 2017, pp. 32–40.

Pedram Johari (Member, IEEE) received the Ph.D. degree in electrical engineering from the University at Buffalo and the State University of New York, Buffalo, NY, USA, in 2018 and the M.B.A. degree from the D'Amore-McKim School of Business, Northeastern University, Boston, MA, USA, 2024, where he has been a Principal Research Scientist with the Institute for Wireless Internet of Things since January 2020. He was a Research Assistant Professor and an Adjunct Lecturer with the University at Buffalo in 2018 and 2019, respectively. He was also the CTO of a startup company on low-power smart IoT devices, NanoThings Inc., New York, from 2018 to 2019. He has collaborated with several academic and industrial research partners, including SUNY Buffalo, Georgia Tech, University of Louisville, Qualcomm, Dell, MathWorks, InterDigital, MITRE, and VIAVI. His current research interests are in the fusion of AI and future generation of cellular networks (5G and beyond), in particular focused on enabling full-protocol digital twins for wireless network systems, Open RAN, spectrum sharing, vehicular communications, and Internet of wireless medical things. In these areas, he is serving as the Lead and Co-PI on multiple grants from U.S. Federal Agencies including the NSF, OUSD(R&E), and NTIA Public Wireless Supply Chain Innovation Funds, as well as multiple industry sponsors. He is the Co-Editor-in-Chief of *Elsevier Software Impacts Journal*, and the Guest Editor of *Elsevier Computer Networks Journal* for the special issue on Digital Twins for Open, Programmable, and AI-driven Wireless Networks. He is a member of ACM

Hadeel Elayan (Member, IEEE) received the Ph.D. degree from the Electrical and Computer Engineering Department, University of Toronto, Canada. She is currently a Postdoctoral Fellow with the Ultrabroadband Nanonetworking Laboratory, Northeastern University, Boston, MA, USA. She holds the Prestigious NSERC Postdoctoral Fellowship from the Canadian Government. He was recognized as an Innovator Under 35 MENA by MIT Technology Review Arabia for her work on THz Induced Protein Interactions. She was named a Rising Star in EECS by the University of Texas at Austin in 2022. Her research interests include nanonetworks, terahertz intra-body communication, and molecular interfaces.

Josep M. Jornet (Fellow, IEEE) received the Degree in telecommunication engineering and the Master of Science degree in information and communication technologies from the Universitat Politècnica de Catalunya, Spain, in 2008, and the Ph.D. degree in electrical and computer engineering from the Georgia Institute of Technology, Atlanta, GA, USA, in August 2013. He is a Professor with the Department of Electrical and Computer Engineering, the Director of the Ultrabroadband Nanonetworking Laboratory, and an Associate Director of the Institute for the Wireless Internet of Things, Northeastern University. From August 2013 to August 2019, he was the Department of Electrical Engineering, University at Buffalo, and The State University of New York. He is a Leading Expert in terahertz communications, in addition to wireless nano-bio-communication networks and the Internet of Nano-Things. In these areas, he has co-authored more than 250 peer-reviewed scientific publications, including one book, and has been granted five U.S. patents. His work has received over 17,000 citations (h-index of 62 as of June 2024). He is serving as the Lead PI on multiple grants from U.S. Federal Agencies including the National Science Foundation, the Air Force Office of Scientific Research, and the Air Force Research Laboratory as well as industry. He is the recipient of multiple awards, including the 2017 IEEE ComSoc Young Professional Best Innovation Award, the 2017 ACM NanoCom Outstanding Milestone Award, the NSF CAREER Award in 2019, the 2022 IEEE ComSoc RCC Early Achievement Award, and the 2022 IEEE Wireless Communications Technical Committee Outstanding Young Researcher Award, and as well as the Four Best Paper Awards. He is a Fellow of IEEE ComSoc Distinguished Lecturer Class from 2022 to 2024. He is also an Editor-in-Chief of the *Elsevier Nano Communication Networks Journal* and an Editor for the IEEE TRANSACTIONS ON COMMUNICATIONS and *Nature Scientific Reports*.